Optical spectroscopy and energy transfer in Tm^{3+}-doped metaphosphate laser glasses

2005 J. Phys.: Condens. Matter 17 4859

(http://iopscience.iop.org/0953-8984/17/32/001)

INSTITUTE OF PHYSICS PUBLISHING JOURNAL OF PHYSICS: CONDENSED MATTER

J. Phys.: Condens. Matter **17** (2005) 4859–4876 doi:10.1088/0953-8984/17/32/001

Optical spectroscopy and energy transfer in Tm^{3+}-doped metaphosphate laser glasses

P Babu[1,4], Hyo Jin Seo[1,5], Kyoung Hyuk Jang[1], R Balakrishnaiah[2], C K Jayasankar[2] and A S Joshi[3]

[1] Department of Physics, Pukyong National University, Pusan 608-737, Korea
[2] Department of Physics, Sri Venkateswara University, Tirupati-509 103, India
[3] High Power Laser Optics Laboratory, Laser Plasma Division, Centre for Advanced Technology, Indore-452 013, India

E-mail: hjseo@pknu.ac.kr

Received 4 June 2005, in final form 4 July 2005
Published 29 July 2005
Online at stacks.iop.org/JPhysCM/17/4859

Abstract

Thulium-doped metaphosphate glasses with four concentrations (0.01, 0.1, 1.0 and 2.0 mol%) of Tm^{3+} have been prepared and investigated by Raman, absorption and photoluminescence spectral studies. The phonon sideband spectrum has been measured for 1.0 mol% Eu^{3+}-doped metaphosphate glass of the same composition and compared with the Raman spectrum. From vibronic spectra, various bands associated with different structural groups have been identified and assigned. Absorption band positions have been used to simulate the complete energy level diagram for the Tm^{3+} ion using the model Hamiltonian. Judd–Ofelt parameters have been determined from the absorption bands. Using these parameters, transition probabilities, excited state lifetimes and transition branching ratios have been evaluated. The emission and decay curves of the $^1D_2$ level have been measured for all four glass samples both at RT and 15 K. Lifetimes show a strong quenching for Tm^{3+} concentrations higher than 0.1 mol%. Fluorescence decay curves of the $^1D_2$ level have been well fitted to the Inokuti–Hirayama model for $S = 6$, suggesting that the mechanism for energy transfer between Tm^{3+} ions is of dipole–dipole type.

1. Introduction

Spectroscopic investigations play a prominent role in characterizing the lanthanide (Ln)-doped materials, which find potential applications in the fields of lasers, optical amplifiers, phosphors, display devices etc, as they allow comprehensive understanding of the various interactions involving radiation and matter. In recent years, there has been a great deal of effort to discover

[4] On leave from: Department of Physics, Government College, Wanaparthy-509 103, India.
[5] Author to whom any correspondence should be addressed.

and develop Tm^{3+}-doped materials for various applications such as in lasers, frequency up-converters and optical amplifiers. The Tm^{3+} ion exhibits emissions at a variety of wavelengths ranging from near infrared to ultraviolet. For example, its $^3F_4 \rightarrow {}^3H_6$ transition is in the range of 1.8–1.9 μm which has applications in medicine and remote sensing of the atmosphere (LIDAR devices) [1, 2]. Another important $^1D_2 \rightarrow {}^3F_4$ transition gives blue emission at ~450 nm in both down- and up-conversions [3–6] which is useful for high capacity data storage optical devices. Similarly, emission of the $^3H_4 \rightarrow {}^3F_4$ transition is used for S-band (1460–1530 nm) amplification (TDFAs) in optical telecommunication [7, 8].

Phosphate glasses are technologically important materials because of their relatively large thermal expansion coefficients, low optical dispersions and low glass transition temperatures [9]. Metaphosphate glasses are used for simultaneous high energy and high peak power laser applications such as the multi-kilojoule and multi-terawatt lasers used for fusion energy research because they have excellent energy storage and extraction characteristics and can be made in large sizes with high optical quality and free of damage-causing inclusions [10]. One disadvantage with the use of phosphate glasses as laser ion hosts is that they have larger thermal expansion and lower fracture toughness than silicates and are more prone to fracture [11]. Though the glass compositions have been developed with good optical properties (suitable for laser action, fibre amplifiers etc), a corresponding quantitative understanding of the relationship between glass structure and performance is still lacking and remains a continuing challenge, giving scope for further investigations in this direction.

The present work reports the spectroscopic properties of Tm^{3+}-doped metaphosphate laser glasses. The base glass composition has been composed from the ranges of different components used in the commercial Nd phosphate laser glass, LG-750 (Schott Glass Technologies) [12]. From the absorption spectrum of 1.0 mol% Tm^{3+}-doped metaphosphate glass (the composition is given in the experimental details section), energy level analysis has been carried out using a free ion model Hamiltonian and radiative properties have been determined using Judd–Ofelt (JO) theory. The Inokuti–Hirayama (IH) model has been applied to decay curves of the $^1D_2$ level at 15 K to derive energy transfer parameters and to explore the nature of the interaction for energy transfer between Tm^{3+} ions.

2. Experimental details

Thulium-doped metaphosphate glasses, with the molar compositions of $(59 - x/2)P_2O_5$–$17K_2O$–$(15 - x/2)BaO$–$9Al_2O_3$–xTm_2O_3 (here after referred to as PKBAT glass) ($x = 0.01$, 0.1, 1.0 and 2.0 mol%) were prepared from appropriate mixtures of reagent-grade $Al(PO_3)_3$, $Ba(PO_3)_2$, KH_2PO_4 and Tm_2O_3 by the melt quenching technique. The batch composition, after thoroughly mixing in an agate mortar, was placed in a platinum crucible and melted in an electric furnace at 1075 °C for about 90 min. The melt was then air quenched by pouring it onto a preheated thick brass plate. The glass samples were annealed at 350 °C for 12 h to remove thermal strains and then allowed to cool to room temperature. The glass samples were well polished for measuring optical properties.

The absorption spectrum was measured using a spectrophotometer (Hitachi U-3400) in the wavelength range of 250–2500 nm. The refractive index, n, was measured using an Abbe refractometer at the sodium wavelength (589.3 nm). The density was measured by the Archimedes method using water as an immersion liquid. The broadband excitation spectrum was measured using a Perkin-Elmer (LS50B) luminescence spectrometer at RT. The Raman spectrum was measured using an FRA 106/s (Bruker, Germany) FT Raman spectrometer at RT. The third-harmonic generation (355 nm) of the Nd:YAG laser (Spectron Laser Sys. SL802G) was used as an excitation source for the photoluminescence (PL) and lifetime measurements.

The fluorescence was dispersed by a 75 cm monochromator (Acton Research Corp. Pro-750), with a resolution of 0.2 nm and observed with a photomultiplier tube (PMT; Hamamtsu R928). The signal from the PMT was fed to a digital oscilloscope (Le Croy 9310) and then the data were stored in a personal computer. Decay curves were obtained using a digital storage oscilloscope interfaced to a personal computer that recorded and averaged the signal. For measurements at 15 K, the sample was cooled in a helium closed-cycle cryostat.

3. Theory

3.1. Energy level analysis

The energy levels of Tm^{3+} are analysed in terms of a parametric free ion Hamiltonian (H_{FI}) which can be written as a sum of six different interactions [13, 14]:

$$H_{FI} = E_{avg} + \sum_{k=2,4,6} F^k f_k + \zeta_{4f} A_{SO} + \alpha L(L+1) + \beta G(G_2) + \gamma G(R_7) + \sum_{j=0,2,4} M^j m_j + \sum_{k=2,4,6} P^k p_k \quad (1)$$

where E_{avg} involves the kinetic energy of the electrons and their interaction with the nucleus. It shifts only the barycentre of the whole 4f configuration. F^k ($k = 2, 4, 6$) are free electron repulsion parameters and ζ_{4f} is the spin–orbit coupling constant. f_k and A_{SO} represent the angular part of the electrostatic and the spin–orbit interaction, respectively. α, β and γ are the Trees interaction parameters. L is the total angular momentum. $G(G_2)$ and $G(R_7)$ are the Casimir operators for the groups G_2 and R_7. M^j ($j = 0, 2, 4$) and P^k ($k = 2, 4, 6$) are magnetic interaction parameters. m_j and p_k represent the operators for the magnetic correction.

Among various interactions, the interelectronic repulsion and the spin–orbit interaction, the second and the third terms, respectively, are the main ones which give rise to the $^{2S+1}L_J$ levels. The rest only make corrections to the energy of these levels without removing their degeneracy.

The parametric fits have been carried out similarly to those in [14], reported for Tm^{3+}:lithium borate glasses. The quality of the parametric fit is generally described in terms of the root mean square (rms) deviation, σ, of the experimental and calculated energies [14] given by

$$\sigma = \sqrt{\frac{\sum_{i=1}^{N} (E_i^{exp} - E_i^{cal})^2}{N}} \quad (2)$$

where E_i^{exp} and E_i^{cal} are the experimental and calculated energies, respectively, for level i and N denotes the total number of levels included in the energy level fit.

3.2. Oscillator strengths—Judd–Ofelt analysis

The JO model [15, 16] describes the absorption and emission properties of f–f transitions of Ln-doped compounds. The experimental oscillator strength (f_{exp}) of an f–f transition in the absorption spectrum can be obtained by means of the expression [17]

$$f_{exp} = 4.32 \times 10^{-9} \int \varepsilon(\upsilon)\, d\upsilon \quad (3)$$

where $\varepsilon(\upsilon)$ is the molar absorptivity at a wavenumber υ cm^{-1}. The theoretical oscillator strength of an f–f transition can be evaluated using the JO theory. In this theory, for an induced

electric dipole transition, the calculated oscillator strength (f_{cal}) for the transition from the ground state to an excited state is given by

$$f_{\mathrm{cal}} = \frac{8\pi^2 mc\upsilon}{3h(2J+1)} \frac{(n^2+2)^2}{9n} \sum_{\lambda=2,4,6} \Omega_\lambda (\Psi J \| U^\lambda \| \Psi' J')^2 \tag{4}$$

where n is the refractive index of the medium, J is the total angular momentum of the ground state, υ is the energy of the transition in cm^{-1}, Ω_λ ($\lambda = 2, 4, 6$) are the JO intensity parameters and $\|U^\lambda\|^2$ are the squared doubly reduced matrix elements of the unit tensor operator of the rank $\lambda = 2, 4$ and 6 which are calculated from the intermediate coupling approximation for the transition $\Psi J \rightarrow \Psi' J'$ [18]. The oscillator strengths of the various observed transitions are evaluated through equation (3) and are used in equation (4). A least squares fitting approximation is then used for equation (4) to determine the Ω_λ parameters which give the best fit between experimental and calculated oscillator strengths. The theoretical oscillator strengths (f_{cal}) are then determined using Ω_λ and equation (4).

3.3. Radiative properties

The radiative transition probability (A) for a transition $\Psi J \rightarrow \Psi' J'$ is calculated from the following equation:

$$A(\Psi J, \Psi' J') = A_{\mathrm{ed}} + A_{\mathrm{md}} \tag{5}$$

where A_{ed} and A_{md} are the electric and magnetic dipole radiative transition probabilities given by

$$\begin{aligned} A_{\mathrm{ed}} &= \frac{64\pi^4 \upsilon^3}{3h(2J+1)} \frac{n(n^2+2)^2}{9} S_{\mathrm{ed}} \\ A_{\mathrm{md}} &= \frac{64\pi^4 \upsilon^3}{3h(2J+1)} n^3 S_{\mathrm{md}} \end{aligned} \tag{6}$$

where S_{ed} and S_{md} are the electric and magnetic dipole line strengths, respectively, calculated from the following expressions [19, 20]:

$$\begin{aligned} S_{\mathrm{ed}} &= e^2 \sum_{\lambda=2,4,6} \Omega_\lambda (\Psi J \| U^\lambda \| \Psi' J')^2 \\ S_{\mathrm{md}} &= \frac{e^2 h^2}{16\pi^2 m^2 c^2} (\Psi J \| L + 2S \| \Psi' J')^2 \end{aligned} \tag{7}$$

and $\frac{n(n^2+2)^2}{9}$ is the local field correction for electric dipole transitions and n^3 for magnetic dipole transitions.

The total radiative transition probability (A_{T}) for an excited state is given as the sum of the $A(\Psi J, \Psi' J')$ terms calculated over all the terminal states:

$$A_{\mathrm{T}}(\Psi J) = \sum A(\Psi J, \Psi' J'). \tag{8}$$

A_{T} is related to the radiative lifetime (τ_{R}) of an excited state by

$$\tau_{\mathrm{R}}(\Psi J) = \frac{1}{A_{\mathrm{T}}(\Psi J)}. \tag{9}$$

The fluorescence branching ratio (β_{R}) corresponding to the emission from an excited ΨJ level to a lower $\Psi' J'$ level can be obtained from the transition probabilities by using

$$\beta_{\mathrm{R}}(\Psi J, \Psi' J') = \frac{A(\Psi J, \Psi' J')}{A_{\mathrm{T}}(\Psi J)}. \tag{10}$$

The peak stimulated emission cross-section, $\sigma(\lambda_p)(\Psi J, \Psi' J')$, for the states ΨJ and $\Psi' J'$ having the probability of $A(\Psi J, \Psi' J')$ can be calculated from

$$\sigma(\lambda_p)(\Psi J, \Psi' J') = \frac{\lambda_p^4}{8\pi c n^2 \Delta\lambda_{eff}} A(\Psi J, \Psi' J') \tag{11}$$

where λ_p is the wavelength of the emission peak and $\Delta\lambda_{eff}$ is the effective linewidth determined by dividing the area of the emission band by its average height.

Equations (5)–(11) have been used to compute various radiative properties.

3.4. Decay curve analysis—Inokuti–Hirayama model

At lower concentrations of dopant Ln ions, where the interaction among the optically active ions is negligible, the fluorescence decay curves can be fitted to a single exponential. However, at higher concentrations Ln ions come closer to each other and the interaction between these ions becomes so prominent that energy transfer takes place from an excited Ln ion (donor) to a non-excited Ln ion (acceptor), leading to a non-exponential shape for the decay curves. The non-exponential shape of these decay curves can fitted to the Inokuti–Hirayama (IH) model [21] to establish the dominant mechanism of interaction. According to this model, the fluorescence decay intensity, I, is given by

$$I(t) = I_0 \exp\left\{-\frac{t}{\tau_0} - Q\left(\frac{t}{\tau_0}\right)^{3/S}\right\} \tag{12}$$

where t is the time after excitation, τ_0 is the intrinsic decay time of the donors in the absence of acceptors. The value of $S = 6$, 8 or 10 depends on whether the dominant mechanism of the interaction is dipole–dipole, dipole–quadrupole or quadrupole–quadrupole, respectively. The energy transfer parameter (Q) is given by

$$Q = \frac{4\pi}{3}\Gamma\left(1 - \frac{3}{S}\right) N_0 R_0^3 \tag{13}$$

and depends at first on S and the gamma function $\Gamma(x)$, which is equal to 1.77 for dipole–dipole ($S = 6$), 1.43 for dipole–quadrupole ($S = 8$) and 1.3 for quadrupole–quadrupole ($S = 10$) interactions. N_0 is the concentration of acceptors, which is almost equal to the total concentration of lanthanide ions, and R_0 is the critical distance defined as a donor–acceptor separation for which the rate of energy transfer to the acceptors is equal to the rate of intrinsic decay of the donor.

If the distance between Ln ions decreases due to increase in concentration, then the Q parameter increases leading to faster fluorescence decays. Equation (12) is valid for the special case of pulsed excitation and a random distribution of optically active ions (donors and acceptors) in the sample. This is because during the pulsed excitation (of the order of a nanosecond) there is not enough time for the donors to transfer the excitation energy to other ions (acceptors).

4. Results

Figure 1 shows the excitation spectrum of the 1.0 mol% Eu^{3+}-doped phosphate glass of similar base composition ($58.5P_2O_5 + 17K_2O + 14.5BaO + 9Al_2O_3 + 1Eu_2O_3$, hereafter referred to as PKBAE glass) to the present Tm^{3+}-doped glasses, measured by monitoring the $^5D_0 \rightarrow {}^7F_2$ emission at 614 nm. The phonon sideband (PSB) spectrum associated with the $^7F_0 \rightarrow {}^5D_2$ transition (the pure electronic band, PEB) of Eu^{3+} ions is clearly observed. The Raman

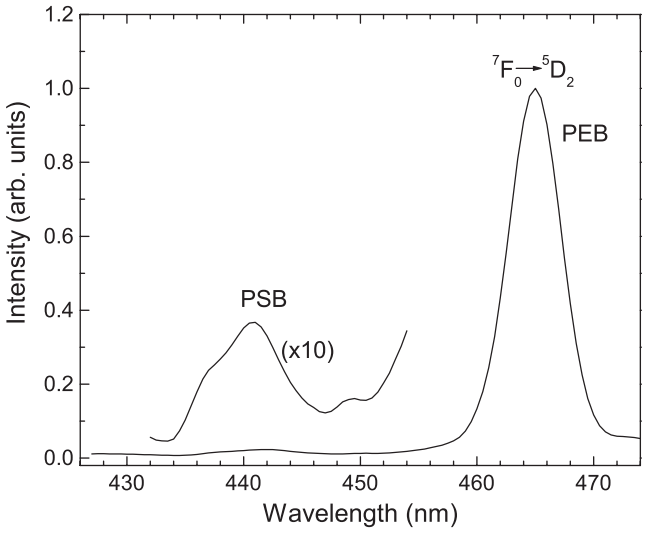

Figure 1. Excitation spectrum of the $^7F_0 \rightarrow {}^5D_2$ transition of Eu^{3+} in the PKBAE glass, monitoring the $^5D_0 \rightarrow {}^7F_2$ emission at 614 nm. The PSB spectrum associated with the PEB is also shown.

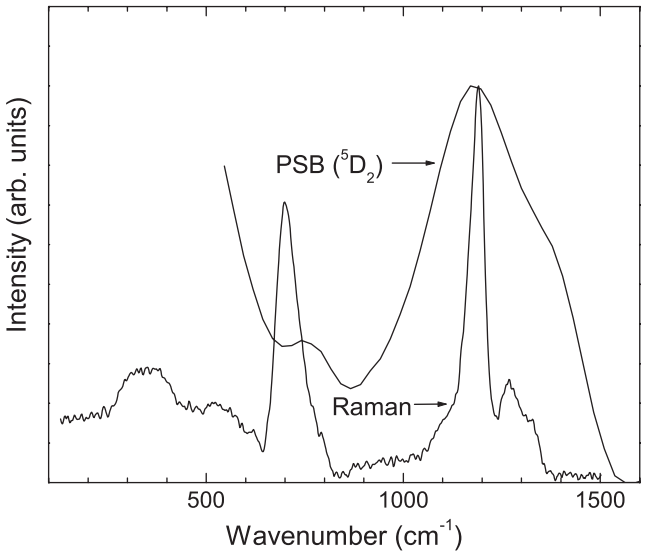

Figure 2. Raman spectrum of 1.0 mol% Tm^{3+}-doped PKBAT glass along with the PSB spectrum associated with the $^7F_0 \rightarrow {}^5D_2$ PEB of Eu^{3+} in the PKBAE glass. Both are normalized with respect to the maximum peak for comparison.

spectrum of the 1.0 mol% Tm^{3+}-doped PKBAT glass is shown in figure 2 along with the PSB spectrum associated with the $^7F_0 \rightarrow {}^5D_2$ PEB. Figure 3 presents the absorption spectrum of the 1.0 mol% Tm^{3+}-doped PKBAT glass at RT in the wavelength range of 300–2100 nm. The experimental energy levels found from the absorption spectrum (barycentres of the bands) are given in table 1. The reported experimental energy levels for some Tm^{3+}-doped systems, that include tellurite [4], fluoroborate [6] glasses, yttrium scandium gallium garnet (YSGG) crystal [22] and aquo-ion [23], are also shown in table 1 for comparison. Free ion parameters

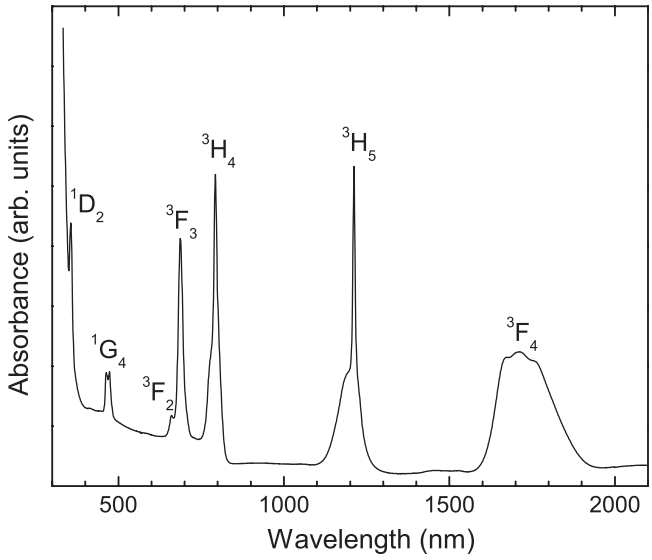

Figure 3. Absorption spectrum of 1.0 mol% Tm^{3+}-doped PKBAT glass. The band assignments are transitions from the ground state, $^3H_6$.

Table 1. Experimental and calculated energies (cm^{-1}) of 1.0 mol% Tm^{3+}-doped PKBAT glass and experimental energies of some reported Tm^{3+}-doped systems.

	PKBAT		Fluoroborate [6]	Tellurite [4]	YSGG [22]	Aquo-ion [23]
Level	Exp.	Cal.	Exp.	Exp.	Exp.	Exp.
$^3H_6$	0	−11	0	0	0	0
$^3F_4$	5 828	5 822	5 988	5 835	5 548	5 730
$^3H_5$	8 251	8 226	8 283	8 383	8 174	8 230
$^3H_4$	12 610	12 643	12 645	12 640	12 489	12 530
$^3F_3$	14 556	14 551	14 893	14 556	14 242	14 330
$^3F_2$	15 152	15 145	15 144	15 166	14 837	14 930
$^1G_4$	21 322	21 318	21 482	21 276	21 049	21 180
$^1D_2$	28 011	28 015	27 956	28 050	27 553	27 830
$^1I_6$	—	35 118	—	—	34 409	34 730
$^3P_0$	—	36 137	—	—	34 941	35 330
$^3P_1$	—	37 056	—	—	35 916	36 230
$^3P_2$	—	38 389	—	—	37 696	38 080
$^1S_0$	—	76 069	—	—	—	—

obtained by minimizing the rms deviation (σ) between experimental and calculated energy levels are collected in table 2. The energy levels calculated with these energy parameters are shown in table 1 for the PKBAT glass.

Energy positions (barycentres) of absorption bands of the 1.0 mol% Tm^{3+}:PKBAT glass, their experimental and calculated oscillator strengths along with reported experimental oscillator strengths for Tm^{3+} ions in fluorophosphate [3], tellurite [4], fluoroindate [5] and fluoroborate [6] glasses are given in table 3. The JO parameters derived for the PKBAT glass are presented in table 4 along with JO parameters for some reported Tm^{3+}:glass systems. From the best fit JO parameters, various radiative properties such as transition probabilities

Table 2. Best fit free ion parameters (cm^{-1}) for Tm^{3+}-doped systems. (Note: the values given in parentheses are the uncertainties in the fitted parameters. The other parameters, $\alpha = 18.19$, $\beta = -745$, $\gamma = 1583$, $M^0 = 7.97$, $M^2 = 0.56M^0$, $M^4 = 0.38M^0$, $P^2 = 982$, $P^4 = 0.75P^2$ and $P^6 = 0.50P^2$, were fixed to the values for Tm^{3+}:$LaCl_3$ [29].)

Parameter	PKBAT	Fluoroborate [6]	Tellurite [4]	YSGG [22]	Aquo-ion [23]
E_{AVG}	18 002(17)	18 099(56)	18 010(22)	17 656(32)	17 819(50)
F^2	103 291(68)	102 093(197)	103 392(86)	101 325(111)	102 487(175)
F^4	75 297(100)	76 558(311)	74 674(126)	71 631(195)	72 973(308)
F^6	50 680(151)	41 489(438)	50 635(191)	52 000(169)	52 837(267)
ζ	−2642(12)	−2654(36)	−2642(15)	−2644(23)	−2646(37)
ΣF^k	229 268	220 140	228 701	224 956	228 297
F^2/F^4	1.37	1.33	1.39	1.42	1.40
F^2/F^6	2.04	2.46	2.04	1.95	1.94
N	8	8	8	12	12
σ	16	49	20	43	68

Table 3. Absorption levels (from the ground state, $^3H_6$), absorption band positions (ν, cm^{-1}), experimental (f_{exp}, $\times 10^{-6}$) and calculated (f_{cal}, $\times 10^{-6}$) oscillator strengths for 1.0 mol% Tm^{3+}-doped PKBAT glass and experimental oscillator strengths for some reported Tm^{3+}:glass systems.

	PKBAT						
Level	ν	f_{exp}	f_{cal}	Fluoro-phosphate [3]	Fluoro-borate [6]	Tellurite [4]	Fluoro-indate [5]
$^3F_4$	5 828	3.03	3.06	2.28	5.62	2.66	1.79
$^3H_5$	8 251	2.00	1.41	1.65	4.50	1.99	1.43
$^3H_4$	12 610	2.28	2.58	2.78	7.09	2.73	1.92
$^3F_3$	14 556	1.56	2.06	2.44[a]	7.88	2.96[a]	2.95[a]
$^3F_2$	15 152	0.20	0.32		1.48		
$^1G_4$	21 322	0.96	0.99	8.4	0.70	8.64	0.70
$^1D_2$	28 011	2.13	2.13	—	1.91	—	1.91

[a] Combined oscillator strengths for $^3F_{2,3}$ transitions.

Table 4. Judd–Ofelt parameters (Ω_λ, $\times 10^{-20}$ cm^2) for 1.0 mol% Tm^{3+}-doped PKBAT glass and for some of the reported Tm^{3+}:glasses.

Glass	Ω_2	Ω_4	Ω_6
PKBAT	5.23	1.95	0.72
Phosphate [30]	8.08	3.05	1.16
Fluorophosphate [3]	5.28	2.32	1.16
Fluoroborate [6]	8.37	3.20	4.34
Tellurite [4]	3.37	1.03	8.51
Fluoroindate [5]	2.36	1.59	1.21
ZBLAN [31]	2.31	1.28	1.17

(A), lifetimes (τ_R) and branching ratios (β_R) have been systematically calculated for all 12 excited levels of Tm^{3+} and are presented in table 5 for the excited levels up to the $^1D_2$ level, to their lower levels, which are normally important for spectroscopic characterization of Tm^{3+}-doped materials for various applications. The predicted radiative lifetimes of the important luminescent transitions, $^1D_2$, $^1G_4$, $^3H_4$ and $^3F_4$, of Tm^{3+}-doped PKBAT glass are shown in table 6 and are compared with similar results for some of the reported Tm^{3+}:glass systems.

Table 5. Emission transitions ($SLJ \rightarrow S'L'J'$), energy gaps (ΔE, cm^{-1}), predicted radiative transition probabilities (A, s^{-1}), branching ratios (β_R) and lifetimes (τ_R, μs) of 1.0 mol% Tm^{3+}-doped PKBAT glass.

SLJ	$S'L'J'$	ΔE	A	β_R	τ_R
$^1D_2$	$^1G_4$	6 689	202	0.008	36
	$^3F_2$	12 859	986	0.037	
	$^3F_3$	13 455	1 182	0.044	
	$^3H_4$	15 401	1 464	0.054	
	$^3H_5$	19 760	63	0.002	
	$^3F_4$	22 183	16 192	0.599	
	$^3H_6$	28 011	6 965	0.257	
$^1G_4$	$^3F_2$	6 170	10	0.005	515
	$^3F_3$	6 766	40	0.021	
	$^3H_4$	8 712	204	0.105	
	$^3H_5$	13 071	521	0.269	
	$^3F_4$	15 494	119	0.061	
	$^3H_6$	21 322	1 044	0.539	
$^3F_2$	$^3F_3$	596	~0	0	876
	$^3H_4$	2 542	16	0.014	
	$^3H_5$	6 901	156	0.136	
	$^3F_4$	9 324	665	0.582	
	$^3H_6$	15 152	305	0.268	
$^3F_3$	$^3H_4$	1 946	4	0.002	582
	$^3H_5$	6 305	342	0.199	
	$^3F_4$	8 728	73	0.042	
	$^3H_6$	14 556	1 299	0.756	
$^3H_4$	$^3H_5$	4 359	24	0.022	932
	$^3F_4$	6 782	102	0.095	
	$^3H_6$	12 610	947	0.883	
$^3H_5$	$^3F_4$	2 423	5	0.025	5365
	$^3H_6$	8 251	182	0.976	
$^3F_4$	$^3H_6$	5 828	240	1	4168

Table 6. Predicted lifetimes (μs) for some important fluorescent levels of 1.0 mol% Tm^{3+}:PKBAT glass and other reported Tm^{3+}:glass systems.

Glass	$^1D_2$	$^1G_4$	$^3H_4$	$^3F_4$
PKBAT	36	515	932	4168
Fluorophosphate [3]	34	454	642	4028
Tellurite [4]	20	330	500	2750
Fluoroborate [6]	20	200	351	2078
Fluoroindate [5]	67	791	1251	7117
ZBLAN [31]	—	764	1396	8490

Emission spectra have been measured both at RT and at 15 K by exciting the PKBAT glass samples with 355 nm (corresponding to the $^1D_2$ level) and the resulting spectra are shown in figures 4 and 5 for RT and 15 K, respectively, for four concentrations (0.01, 0.1, 1.0 and 2.0 mol%) of Tm^{3+} ions. From the measured emission spectra at RT and 15 K, emission peak positions (λ_p), effective linewidths ($\Delta\lambda_{eff}$), experimental branching ratios (relative areas under the emission bands) and stimulated emission cross-sections ($\sigma(\lambda_p)$) of the $^1D_2 \rightarrow {}^3F_4$ and

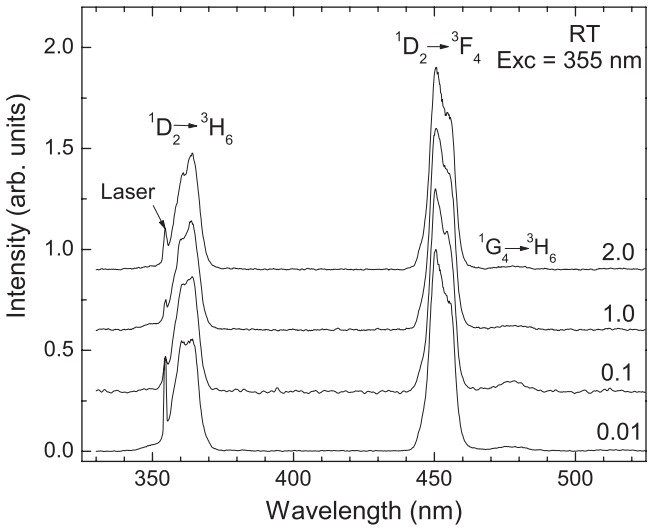

Figure 4. Normalized emission spectra of Tm^{3+}:PKBAT glasses (λ_{exc} = 355 nm) for different concentrations (mol%) of Tm^{3+} ions at RT. Emission band assignments are also shown.

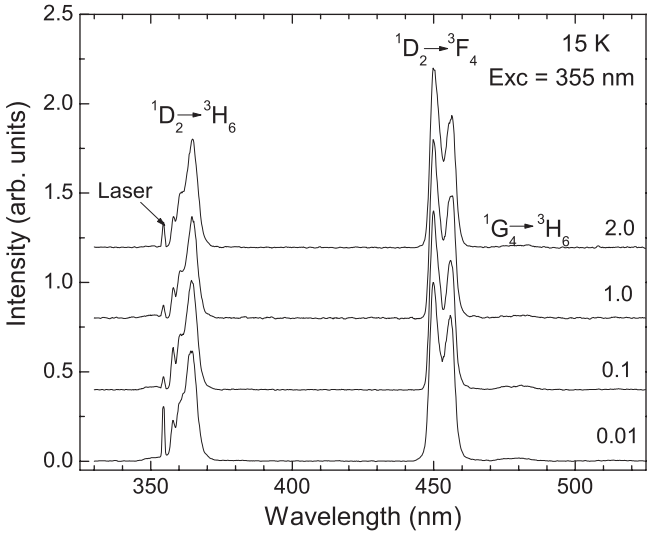

Figure 5. Normalized emission spectra of Tm^{3+}:PKBAT glasses (λ_{exc} = 355 nm) for different concentrations (mol%) of Tm^{3+} ions at 15 K. Emission band assignments are also shown.

$^3H_6$ transitions have been evaluated and are presented in table 7 for 1.0 mol% Tm^{3+}-doped PKBAT glass.

Decay curves of the $^1D_2$ level for four Tm^{3+}:PKBAT glasses have been measured at both RT and 15 K under 355 nm excitation by monitoring the $^1D_2 \rightarrow {}^3F_4$ transition (452 nm) and are shown in figure 6 for 15 K. From these decay curves, lifetimes of the $^1D_2$ level have been determined by finding the first e-folding times and these are presented in table 8. The quantum efficiency of the $^1D_2$ level of Tm^{3+} has been evaluated for four Tm^{3+}:PKBAT glasses and the results are given in table 8. The energy transfer parameter (Q) has been obtained from the

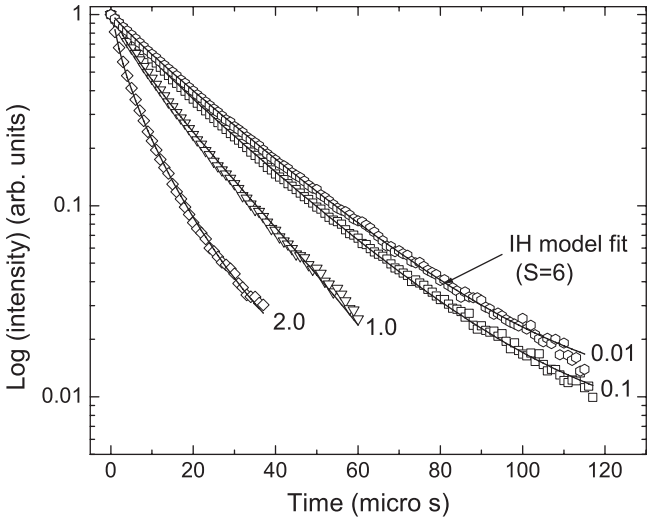

Figure 6. Decay curves of the $^1D_2$ level for different concentrations (mol%) of Tm^{3+}-doped PKBAT glasses at 15 K ($\lambda_{exc} = 355$ nm). The solid line indicates the IH model fitting for $S = 6$.

Table 7. Emission peak positions (λ_p), effective linewidths ($\Delta\lambda_{eff}$), experimental and calculated branching ratios (β_R) and stimulated emission cross-sections ($\sigma(\lambda_p)$) of $^1D_2 \rightarrow {}^3F_4$ and $^3H_6$ transitions of 1.0 mol% PKBAT glass at RT and 15 K.

					β_R				
	λ_p (nm)		$\Delta\lambda_{eff}$ (nm)		Exp.			$\sigma(\lambda_p)$ ($\times 10^{-20}$ cm^2)	
Transition	RT	15 K	RT	15 K	RT	15 K	Cal	RT	15 K
$^1D_2 \rightarrow {}^3F_4$	452	453	7.64	7.82	0.65	0.69	0.60	4.89	4.82
$^1D_2 \rightarrow {}^3H_6$	362	364	7.85	5.52	0.35	0.31	0.26	0.84	1.22

Table 8. Experimental lifetimes (τ_{exp}) and quantum efficiencies (η) of the $^1D_2$ level, energy transfer parameters (Q) and critical distances (R_0) for different concentrations (mol%) of Tm^{3+}-doped PKBAT glasses at RT/15 K.

Conc.	τ_{exp} (μs)	η	Q	R_0 (Å)
0.01	21	58	0.23	23
0.1	19	53	0.38	13
1.0	12	33	0.91	8
2.0	5	14	2.33	9

process of fitting to the decay curve of the $^1D_2$ level which in turn has been used to calculate the critical distance (R_0) using equation (13). The values of Q and R_0 are also shown in table 8 for four concentrations of Tm^{3+}:PKBAT glasses.

5. Discussion

5.1. Vibronic spectra

Phonon sideband (PSB) spectra are useful for investigating the local structure surrounding Ln ions in the glass matrix. The difference between the position of the PEB and the PSB

corresponds to the energy of phonons coupled to the electronic levels of Ln ions. The PSB spectrum of figure 1, measured for the PKBAE glass, consists of one weak band at around 770 cm^{-1}, an intense broad band at around 1180 cm^{-1} and a weak overlapped band near 1340 cm^{-1}. The weak PSB at around 770 cm^{-1} is due to coupling of P–O–P asymmetric stretching vibrations of the PO_2 group [24]; the PSBs near 1180 and 1340 cm^{-1} are caused by the coupling of symmetric and strained asymmetric stretching vibrations of the PO_2 groups, respectively, to the electronic levels of Eu^{3+} ions. Similar results for the PSB spectrum were also noted for $Sr(PO_3)_2$–$Eu(PO_3)_3$ metaphosphate glass [25]. The electron–phonon coupling strength (g) is given by intensity ratio of the PSB to the PEB. For the PKBAE glass, the value of g for an intense, broad and overlapped PSB is found to be 0.054 which is nearly three times larger than the value obtained for the $Sr(PO_3)_2$–$Eu(PO_3)_3$ metaphosphate glass [25].

Metaphosphate glasses have Q^2 polymerization structure for the $(PO_4)^{-1}$ tetrahedron, with two bridging and two non-bridging oxygens (NBOs) [24]. Raman spectra of the metaphosphate glasses provide information about the interaction between the metal cation and the PO_2 group [26]. As can be seen from figure 2, the PSB spectrum corresponds well with the Raman spectrum.

The Raman spectrum of PKBAT glass, shown in figure 2, consists of two strong bands at around 700 and 1190 cm^{-1}, which are normally observed for metaphosphate glasses [26, 27], and a weak band near 1260 cm^{-1} with a shoulder at around 1330 cm^{-1}. The band at 700 cm^{-1} is also associated with a shoulder near 780 cm^{-1}. A broad band at around 340 cm^{-1} is assigned to PO_2 and in-chain O–P–O bending and torsional vibrations [24, 27]. The band at around 700 cm^{-1} is assigned to symmetrical stretching vibrations of P–O–P linkages [26, 28]. The high frequency shoulder ($\sim$780 cm^{-1}) associated with this band is caused by P–O–P asymmetric stretching vibrations of the PO_2 group [24]. The most intense band near 1190 cm^{-1} is due to the $(PO_2)_{sym}$ stretching mode of non-bridging terminal oxygens (P=O and P–O^-) in Q^2 metaphosphate tetrahedra [24], where the π-bonding is delocalized over the two equivalent P–NBO bonds resulting in each having a bond order of $\sim$1.5. The $(PO_2)_{sym}$ Raman band at 1190 cm^{-1} of PKBAT glass is in good agreement with the Raman spectral data for binary metaphosphate glasses containing the cations K^+, Ba^{2+} and Al^{3+} [26]. The weak band appearing near 1260 cm^{-1} is assigned to asymmetric stretching vibrations of PO_2 (terminal P–O bonds) [24, 28]. A high frequency shoulder associated with this band near 1330 cm^{-1} is due to strained asymmetric stretching vibration of PO_2 groups [24].

Comparison of Raman and PSB spectra reveals that intense phonon bands are caused by the vibrations with the greatest phonon energy. Thus these phonons of PO_2 groups in metaphosphate glasses are mainly responsible for multiphonon relaxation.

5.2. Energy level analysis

Using the experimental energy positions of excited states of Tm^{3+}, obtained from the absorption spectrum, energy level analyses have been carried out for the PKBAT glass and for some of the reported Tm^{3+}-doped systems shown in table 1, to determine the best fit free ion parameters using equations (1) and (2) by the least squares fit method. Calculations have been performed by diagonalizing the total atomic Hamiltonian within the complete $f^{12}SLJ$ basis set comprising 13 SLJ multiplets of the f^{12} (Tm^{3+}) configuration. During these energy level fits, only the atomic parameters F^k ($k = 2, 4$ and 6) and ζ were freely varied, the other parameters, α, β, γ, M^j and P^k, being kept fixed to the values for Tm^{3+}:$LaCl_3$ [29] (shown in the note of table 2). Four of these parameters, M^2, M^4, P^4 and P^6, were restricted according to $M^2 = 0.56M^0$, $M^4 = 0.38M^0$, $P^4 = 0.75P^2$ and $P^6 = 0.50P^2$ [14]. The starting parameters for the fits were also taken from the values for Tm^{3+}:$LaCl_3$. The sum of the repulsive Coulomb parameters

($\sum_k F^k$), hydrogenic ratios, F^2/F^4 and F^2/F^6, along with σ and the number of experimental levels (N) used in the fit, are presented in table 2 for PKBAT glass and for reported Tm^{3+}-doped systems.

From table 1, it can be found that the simulation of energy levels for Tm^{3+}-doped PKBAT glass is quite reasonable, with a small rms deviation of 16 cm^{-1} confirming that the interelectronic and the spin–orbit interactions are mainly responsible for the energy level diagram of the Tm^{3+} ion. The free ion parameters shown in table 2 for PKBAT glass and other reported Tm^{3+}-doped systems are consistent with the values reported in [14] for various Tm^{3+}-doped systems. Among glass systems, fluoroborate glass shows a large rms deviation of 49 cm^{-1}. As can be seen from table 2, the magnitudes of the atomic parameters of glasses are more or less similar to those observed for YSGG crystal and aquo-ion systems. This feature is a consequence of the relatively weak influence of the local environment on the energy level positions of $^{2S+1}L_J$ multiplets because of the shielding of 4f electrons by the $5s^2$ and $5p^6$ electrons. From the values of ($\sum_k F^k$), for the systems shown in table 2, it can be said that the net electrostatic field experienced by the Tm^{3+} ion is maximum in PKBAT glass and minimum in fluoroborate glass whereas it is moderate in tellurite glass, YSGG crystal and the aquo-ion system. Though the hydrogenic ratios appear to be more or less similar, F^2/F^4 slightly increases from 1.39 (glass) to 1.42 (crystal) and F^2/F^6 decreases from 2.04 (glass) to 1.95 (crystal). Similar results for hydrogenic ratios has also been reported by Jayasankar and Renuka Devi [14] for different Tm^{3+}-doped systems. The free ion parameters given in table 2 can be used to construct exact wavefunctions for calculating more accurate and appropriate matrix elements for respective systems for use in the JO analysis.

5.3. Judd–Ofelt analysis and radiative properties

In the absorption spectrum of figure 3, each absorption peak corresponds to the transition from the ground state, $^3H_6$, to the excited state of the Tm^{3+} ion. The absorption bands are assigned based on the Tm^{3+}:aquo-ion [23] energy level diagram and reported absorption spectra of Tm^{3+}:glass systems [3–6]. All the observed absorption bands are pure electric dipole in nature except the $^3H_6 \rightarrow {}^3H_5$ one, which contains a large electric dipole and very small magnetic dipole contribution. From the absorption spectrum, experimental oscillator strengths have been determined using equation (3), and by using equation (4) JO analysis has been carried out by the least squares fitting method to obtain the best fit JO intensity parameters (Ω_λ, $\lambda = 2, 4, 6$) with minimum rms deviation (equation (2)) between experimental and calculated oscillator strengths. The overlapping $^3F_2$ and $^3F_3$ peaks have been separated into two independent ones by using the Gaussian fit method for the estimation of experimental oscillator strengths.

From table 3, the oscillator strengths of 1.0 mol% Tm^{3+}-doped PKBAT glass are comparable to those of fluoroindate glass whereas those of fluorophosphate and tellurite glasses are of the same order of magnitude. Among the Tm^{3+}:glass systems compared in table 3, fluoroborate glass has larger values of the oscillator strengths. It is interesting to note, from table 4, that the order of the JO parameters ($\Omega_2 > \Omega_4 > \Omega_6$) is same for PKBAT, phosphate [30], fluorophosphate, ZBLAN [31] and fluoroindate glasses, whereas it differs for fluoroborate and tellurite glasses—in particular, the order of Ω_2 and Ω_6 is reversed for these latter two systems. Among the JO parameters, Ω_2 is sensitive to both asymmetry and covalency at the Ln ion sites [32] and Ω_4 and Ω_6 reflect the bulk properties of the glasses [33]. Since the f–f transitions of Ln ions are parity forbidden, deviations from inversion symmetry give rise to an increase of the Ω_2 values [34]. Changes of Ω_2 are due to changes of asymmetry and covalency between Ln ions and ligand anions [35]. Among the Tm^{3+}:glass systems compared in table 4, oxide (phosphate) and oxyfluoride (fluorophosphates and fluoroborate) glasses have

larger values of Ω_2 than pure fluoride (ZBLAN), fluoroindate and tellurite glasses, indicating that the asymmetry at the Tm^{3+} ion site and the Tm–O covalency are larger in the former glasses.

From table 6, it is interesting to note that the lifetimes predicted for Tm^{3+}:PKBAT glass are nearer to those for fluorophosphate [3] glass. Moreover, predicted lifetimes for phosphate and fluorophosphate glasses are nearly two times larger than those for tellurite [4] and fluoroborate [6] glasses and are intermediate between those for oxide/oxyfluoride (tellurite and fluoroborate) and fluoride (fluoroindate [5] and ZBLAN [31]) glasses. Among the Tm^{3+}:glass systems compared in table 6, fluoroindate and ZBLAN glasses possess more or less similar predicted lifetimes (except for the $^3F_4$ level, where the difference is slightly larger) and are larger than those for other Tm^{3+}:glass systems shown in table 6.

5.4. Fluorescence properties

Emission spectra for the title glasses, shown in figures 4 and 5, consist of two strong bands at ∼363 nm and ∼452 nm which are assigned to $^1D_2 \rightarrow {}^3H_6$ and $^1D_2 \rightarrow {}^3F_4$ transitions, respectively, and a weak band at ∼479 nm corresponds to the $^1G_4 \rightarrow {}^3H_6$ transition. The latter weak transition is caused by the small non-radiative decay due to multiphonon relaxation from the main $^1D_2$ fluorescent level. The observation and intensities of the transitions originating from the $^1D_2$ level are in accordance with the JO theory which predicts relatively large branching ratios (table 5) for these transitions, with a maximum of ∼0.6 for the $^1D_2 \rightarrow {}^3F_4$ transition. As can be seen from figures 4 and 5, the intensity of the $^1G_4 \rightarrow {}^3H_6$ transition increases with concentration from 0.01 to 0.1 mol% and then decreases.

The emission parameters such as λ_p, $\Delta\lambda_{eff}$, experimental and calculated β_R and $\sigma(\lambda_p)$ are collected in table 7 for both RT and 15 K for 1.0 mol% Tm^{3+}:PKBAT glass. The values for other concentrations are more or less similar. As can be seen from table 7, $\Delta\lambda_{eff}$ and $\sigma(\lambda_p)$ values for the $^1D_2 \rightarrow {}^3F_4$ transition are more or less similar at RT and 15 K. It is worth noting that the emission properties of the $^1D_2 \rightarrow {}^3F_4$ transition, except the lifetime, are unaffected by the changes in temperature and concentration of Tm^{3+} ions. Slightly higher values of $\Delta\lambda_{eff}$ and β_R for the $^1D_2 \rightarrow {}^3H_6$ transition at RT are caused by overlapping of the laser peak (355 nm). In some cases, for example for 0.01 mol% emission, it was possible to deconvolute the laser peak, but in other cases this was found difficult. From table 7, it can be found that experimental branching ratios are comparable with those calculated from the JO theory. At 15 K, relatively large branching ratios are noted for the $^1D_2 \rightarrow {}^3F_4$ transition. But these values (∼0.69) are less than the experimental β_R (0.89) noted in the case of Tm^{3+}-doped fluoroborate glass [6]. As expected, the stimulated emission cross-section is higher for the $^1D_2 \rightarrow {}^3F_4$ transition and is almost independent of temperature.

The lifetime of the Ln^{3+} ion excited state in a glass matrix is governed by radiative and non-radiative processes. The non-radiative processes can be due to multiphonon relaxation and energy transfer between Ln^{3+} ions. The probability of multiphonon relaxation depends on the phonon energy of the host matrix while the energy transfer processes are influenced by the Ln^{3+} ion concentration. Hence, the lifetime of the Ln^{3+} ion excited state can be expressed as [3]

$$\frac{1}{\tau} = \frac{1}{\tau_R} + W_{MP} + W_{ET} \tag{14}$$

where τ is the measured lifetime, τ_R is the radiative lifetime determined from the JO theory, W_{MP} is the probability of multiphonon relaxation and W_{ET} is the probability of energy transfer among neighbour Ln^{3+} ions.

In the case of PKBAE glass, the highest phonon energy band is at around 1340 cm^{-1} (from the PSB spectrum of figure 2) and the energy gap between the $^1D_2$ and $^1G_4$ levels in PKBAT glass is ∼6690 cm^{-1}; hence, it needs around five phonons to bridge the energy gap. Therefore, non-radiative decay due to multiphonon relaxation is present in PKBAT glasses but its magnitude is small. This is evident from the weak $^1G_4 \rightarrow {}^3H_6$ band (figures 4 and 5) which is the most probable transition from the $^1G_4$ level with a branching ratio of ∼0.54 (table 5). In the case of 0.01 mol% Tm^{3+}:PKBAT glass, where the energy transfer between Tm^{3+} ions is negligible, W_{MP} ($^1D_2$) is found to be 19 841 s^{-1} (from equation (14)). The error in this value is subjected to the approximations in the JO theory. This value of W_{MP} is very much less than that (192 810 s^{-1}) obtained in the case of Tm^{3+}-doped tungstate fluorophosphate glasses [3], where a large deviation between experimental (4.5 μs) and calculated (34 μs) lifetimes has been noted.

The decay curves of the $^1D_2$ level obtained at 15 K, shown in figure 6, are found to be non-exponential for all four concentrations and a similar behaviour is noted at RT also. As can be seen from figure 6, the non-exponential nature of the decay curves increases with increase in concentration of Tm^{3+} ions. It is worth noting that the lifetimes of the $^1D_2$ level are the same at RT and 15 K which clearly indicates that the lifetime is independent of temperature. But the lifetime decreases rapidly with increase in concentration (from 21 μs for 0.01 mol% to 5 μs for 2.0 mol% Tm^{3+}:PKBAT glass). The decrease in the $^1D_2$ level lifetime, along with increase of the non-exponential nature for the decay curves, clearly indicates enhancement of the processes of energy transfer between nearby Tm^{3+} ions with increase in Tm^{3+} concentration.

We propose two probable cross-relaxation mechanisms for the energy transfer between Tm^{3+} ions to account for the observed lifetime quenching of the $^1D_2$ level associated with an increase in the non-exponential nature for the decay curves as well as for the change in intensity of the $^1G_4 \rightarrow {}^3H_6$ emission band with increase in Tm^{3+} concentration. The first one, $^1D_2 + {}^3H_6 \rightarrow {}^1G_4 + {}^3F_4$ (which depopulates the $^1D_2$ level and populates the $^1G_4$ level) is almost resonant with a mismatch of about 860 cm^{-1} which can be bridged by the emission of one P–O phonon (∼770 cm^{-1}) and inhomogeneous broadening of the levels. The second one, $^1G_4 + {}^3H_6 \rightarrow {}^3F_{2,3} + {}^3F_4$ (which depopulates the $^1G_4$ level) [6] is also resonant with a mismatch of 340 cm^{-1} which can be bridged by the emission of one O–P–O bending phonon (340 cm^{-1}). It seems to be reasonable to assume that at lower Tm^{3+} concentrations (0.01–0.1 mol%), the first cross-relaxation mechanism is weak, dominant and increases with concentration, as evidenced from the small decrease of the $^1D_2$ level lifetime (2 μs), presence and small increase in the non-exponential nature for the decay curve and increase in intensity of the $^1G_4 \rightarrow {}^3H_6$ emission band for 0.1 mol% Tm^{3+} concentration. With increase in the Tm^{3+} concentration (from 0.1 to 2.0 mol%), the strength of both the above cross-relaxation energy transfer processes, between Tm^{3+} ions, increases as evidenced by the strong quenching of the $^1D_2$ level lifetime (from 19 to 5 μs) associated with enhanced non-exponential nature for the decay curves and decrease in intensity of the $^1G_4 \rightarrow {}^3H_6$ emission band.

The luminous quantum efficiency (η) is defined as the ratio of the number of photons emitted to the number of photons absorbed. For Ln^{3+} ion systems, it is equal to the ratio of the measured lifetime to the calculated lifetime for respective levels given by [12, 36]

$$\eta = \frac{\tau_{meas}}{\tau_{calc}} \times 100. \tag{15}$$

The value of η is found to decrease from 58 to 14 when the concentration of Tm^{3+} is increased from 0.01 to 2.0 mol%. Phonon-assisted cross-relaxation energy transfer between nearby Tm^{3+} ions appears to be mainly responsible for the observed decrease in quantum efficiency of the $^1D_2$ level with increase in the concentration of Tm^{3+} ions in PKBAT glasses.

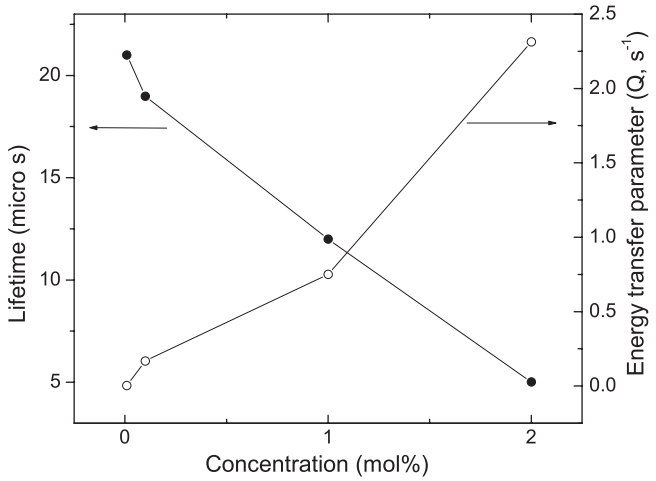

Figure 7. Variation of the lifetime of the $^1D_2$ level and energy transfer parameter (Q) versus Tm^{3+} concentration (mol%) in PKBAT glasses.

To explore the nature of the mechanism for energy transfer between Tm^{3+} ions in PKBAT glasses, decay curves of the $^1D_2$ level at 15 K have been fitted to the IH model [21] (equation (12)). Best fits of the experimental decay curves have been obtained for $S = 6$ (shown in figure 6) which clearly indicate that the dominant interaction for energy transfer between Tm^{3+} ions is of dipole–dipole type. Since the decay curve of the $^1D_2$ level for 0.01 mol% Tm^{3+}:PKBAT glass is also non-exponential, the intrinsic lifetime τ_0 (where there is no energy transfer) was obtained by freely varying the τ_0 value also for best fit during fitting (with $S = 6$) of the decay curve for 0.01 mol% Tm^{3+}:PKBAT glass. This value of τ_0 (26 μs) has been fixed for subsequent fittings of the decay curves for 0.1–2.0 mol% Tm^{3+}:PKBAT glasses. Jerez *et al* [5] also noted dipole–dipole interaction as the mechanism for energy transfer between Tm^{3+} ions in fluoroindate glasses while analysing the 455 nm emission from the $^1D_2$ level through the IH model. They considered the lifetime derived from the JO theory as an intrinsic lifetime for fitting decay curves. This may be reasonable for fluoroindate glass because of its lower phonon energy ($\sim$500 cm^{-1}), which makes the multiphonon relaxation from the $^1D_2$ level negligible. In the case of PKBAT glasses, when the lifetime obtained from the JO theory (36 μs) was used as an intrinsic lifetime, the fitting of the decay curves showed a large deviation. This may be because of the presence of a considerable non-radiative decay due to multiphonon relaxation in PKBAT glasses.

The values of the energy transfer parameter (Q) obtained in the fitting process for the decay curves of the $^1D_2$ level, shown in table 8, increases from 0.23 to 2.33 with increase in the Tm^{3+} concentration from 0.01 to 2.0 mol%. As can be seen from figure 7 and table 8, lifetimes and Q values follow opposite trends with increase in concentration of Tm^{3+} ions, strongly indicating the lifetime quenching behaviour of energy transfer processes.

The value of R_0, calculated from the fitting parameter, Q, first decreases from 23 to 8 Å with increase in the Tm^{3+} concentration (from 0.01 to 1.0 mol%) and then becomes almost constant (9 Å for 2.0 mol%). The change in the R_0 value with the Tm^{3+} concentration in PKBAT glasses is rather puzzling. In fact, R_0 should be independent of the Tm^{3+} concentration as it depends only on the strength of the donor–acceptor coupling. The change in the R_0 value may be due to the onset of energy migration among the donors at relatively high Tm^{3+} concentrations. It is interesting to note that in the case of PKBAT glasses, the decrease in the R_0 value

with the increase in the Tm^{3+} concentration from 0.01 to 1.0 mol% is similar to the trend of R_0 values found for Tb^{3+}–Tm^{3+} co-doped lead silicate glasses with increase in the Tm^{3+} concentration [37], and the near constancy of the R_0 values found for higher concentrations of Tm^{3+} (1.0 and 2.0 mol%) is similar to the behaviour of the R_0 values observed for Tm^{3+}-doped fluoroindate glasses [5].

From the behaviour of emission spectra, lifetimes and critical distances (R_0) for energy transfer, it can be concluded that phonon-assisted cross-relaxation processes of energy transfer between excited Tm^{3+} ions (donors) and ground state Tm^{3+} ions (acceptors) are mainly responsible for the observed non-radiative energy transfer in Tm^{3+}:PKBAT glasses. At higher concentrations (>1.0 mol%), energy migration [38], which involves resonant energy transfer among the donors and finally to an impurity such as a transition metal ion or some other quenching centre in the glass, may also be a contributing factor for lifetime quenching of the $^1D_2$ level. Increase in the slope of energy transfer parameter versus concentration graph (figure 7) after 1.0 mol% supports this assumption.

6. Conclusions

Thulium-doped metaphosphate glasses with four concentrations of Tm^{3+} have been investigated through vibronic, absorption and photoluminescence spectral studies. Comparison of the Raman and phonon sideband spectra (measured for PKBAE glass) reveals that intense phonon bands are caused by the vibrations with greatest phonon energy which are due to PO_2 groups in metaphosphate glasses. The simulated energy level diagram of Tm^{3+} ions in PKBAT glass using the model Hamiltonian is reasonably good, with a minimum rms deviation of 16 cm^{-1}. The value of the JO parameter, Ω_2, for the PKBAT glass, which indicates asymmetry at the Tm^{3+} ion site and Tm–O covalency, is intermediate between those for fluoroborate and fluoride glasses. The radiative properties predicted, using the JO theory, for Tm^{3+} fluorescent levels in 1.0 mol% Tm^{3+}:PKBAT glass are in good agreement with the experimental values. The energy gap between $^1D_2$ and $^1G_4$ levels in PKBAT glasses is found to be equivalent to around five phonons, which indicates the presence of a small non-radiative decay due to the multiphonon relaxation between them. The decrease in quantum efficiency and increase in non-exponential nature for the decay curves of the $^1D_2$ level are due to an increase in the strength of the phonon-assisted cross-relaxation processes of energy transfer between Tm^{3+} ions with increase in the Tm^{3+} concentration. The non-exponential decay curves of the $^1D_2$ level, observed for all four concentrations of Tm^{3+} ions, are well fitted to the Inokuti–Hirayama model for $S = 6$, indicating that the interaction for energy transfer between Tm^{3+} ions is of dipole–dipole nature.

Acknowledgments

This work was supported by KRF (Grant No KRF-2002-070-C00042). The authors CKJ and ASJ are grateful to DAE-BRNS, Government of India, for sanctioning the major research project No 2003/34/4-BRNS/600.

References

[1] Hollis D B, Cruickshank F R and Payne M J P 2001 *J. Non-Cryst. Solids* **293–295** 422
[2] Braud A, Tigreat P Y, Doualan J L and Moncorge R 2001 *Appl. Phys.* B **72** 909
[3] Poirier G, Jerez V A, de Araujo C B, Messaddeq Y, Ribeiro S J L and Poulain M 2003 *J. Appl. Phys.* **93** 1493
[4] Poirier G, Cassanjes F C, de Araujo C B, Jerez V A, Ribeiro S J L, Messaddeq Y and Poulain M 2003 *J. Appl. Phys.* **93** 3259

[5] Jerez V A, de Araujo C B and Messaddeq Y 2004 *J. Appl. Phys.* **96** 2530
[6] Lim K S, Babu P, Jayasankar C K, Lee S K, Pham V T and Seo H J 2004 *J. Alloys Compounds* **385** 12
[7] Aitken B G, Dejneka M J and Powley M L 2004 *J. Non-Cryst. Solids* **349** 115
[8] Yamauchi H, Murugan G S and Ohishi Y 2004 *J. Appl. Phys.* **96** 7212
[9] Kirkpatrick R J and Brow R K 1995 *Solid State Nucl. Magn. Reson.* **5** 9
[10] Ehrmann P R, Carlson K, Campbell J H, Click C A and Brow R K 2004 *J. Non-Cryst. Solids* **349** 105
[11] Suratwala T I, Steele R A, Wilke G D, Campbell J H and Takeuchi K 2000 *J. Non-Cryst. Solids* **263/264** 213
[12] Campbell J H and Suratwala T I 2000 *J. Non-Cryst. Solids* **263/264** 318
[13] Wybourne B G 1965 *Spectroscopic Properties of Rare Earths* (New York: Interscience)
[14] Jayasankar C K and Renuka Devi A 1996 *Opt. Mater.* **6** 185
[15] Judd B R 1962 *Phys. Rev.* **127** 750
[16] Ofelt G S 1962 *J. Chem. Phys.* **37** 511
[17] Gorller-Walrand C and Binnemans K 1998 *Hand Book on the Physics and Chemistry of Rare Earths* vol 25, ed K A Gschneidner Jr and L Eyring (Amsterdam: North-Holland) chapter 167
[18] Rukmini E and Jayasankar C K 1994 *J. Non-Cryst. Solids* **176** 213
[19] Carnall W T, Fields P R and Wybourne B G 1965 *J. Chem. Phys.* **42** 3792
[20] Weber M J, Ziegler D C and Angell C A 1982 *J. Appl. Phys.* **53** 4344
[21] Inokuti M and Hirayama F 1965 *J. Chem. Phys.* **43** 1978
[22] Seltzer M D, Gruber J B, Hills M E, Quaries G J and Morrison C A 1993 *J. Appl. Phys.* **74** 2821
[23] Carnall W T, Fields P R and Rajnak K 1968 *J. Chem. Phys.* **49** 4424
[24] Hudgens J J, Brow R K, Tallant D R and Martin S W 1998 *J. Non-Cryst. Solids* **223** 21
[25] Ebendorff-Heidepriem H and Ehrt D 1996 *J. Non-Cryst. Solids* **208** 205
[26] Nelson B N and Exarhos G J 1979 *J. Chem. Phys.* **71** 2739
[27] Ilieva D, Jivov B, Bogachev G, Petkov C, Penkov I and Dimitiev Y 2001 *J. Non-Cryst Solids* **283** 195
[28] Poirier G, Messaddeq Y, Ribeiro S L and Poulain M 2005 *J. Solid State Chem.* **178** 1533
[29] Jayasankar C K, Richardson F S and Reid M F 1989 *J. Less-Common Met.* **148** 289
[30] Spector N, Reisfeld R and Boehm L 1977 *Chem. Phys. Lett* **49** 49
[31] Doualan J L, Girard S, Haquin H, Adam J L and Montagne J 2003 *Opt. Mater.* **24** 563
[32] Reisfeld R 1975 *Struct. Bonding* **22** 123
[33] Nageno Y, Takebe H and Morinaga K 1993 *J. Am. Ceram. Soc.* **76** 3081
[34] Reisfeld R 1973 *Struct. Bonding* **13** 53
[35] Ebendorff-Heidepriem H, Ehrt D, Bettinelli M and Speghini A 1998 *J. Non-Cryst. Solids* **240** 66
[36] Pisarski W A 2005 *J. Mol. Struct.* **744–747** 473
[37] Bettinelli M and Ingletto G 1989 *J. Lumin.* **43** 115
[38] Weber M J 1971 *Phys. Rev.* B **4** 2932